Molecular dynamics study of cluster evolution in supersaturated vapor

D. I. Zhukhovitskii
Institute for High Temperatures, Russian Academy of Sciences, Izhorskaya, 13/19, 127412 Moscow, Russia

(Received 15 May 1995; accepted 30 August 1995)

Behavior of an argonlike cluster in supersaturated vapor at constant temperature and pressure is simulated. In contrast to the results of conventional microcanonical ensemble simulations, instability of cluster size is observed (unlimited growth or complete evaporation). This defines cluster critical size, which is noticeably larger than that predicted by the classical nucleation theory. Analysis of cluster collective vibrational spectra shows that its evaporation is intimately connected with spontaneous emergence of the lowest modes of breathing vibrations. The cluster phonon spectrum resembles that of a strange attractor. © *1995 American Institute of Physics.*

I. INTRODUCTION

Each theory of homogeneous nucleation, from the classical nucleation theory[1–4] to its modern improved versions[5–8] is associated with a number of axiomatic assumptions. Although computer simulation is a powerful tool for *ab initio* calculations, a straightforward simulation of nucleation is impossible, because computer resources impose a severe constraint on the number of particles in a system. As a result, every attempt of computer simulation implies principle simplifications, e.g., space dimensionality reduction,[9] which yields rather qualitative results. Numerous studies of a single cluster in equilibrium with vapor environment were carried out for the Gibbs microcanonical ensemble (the total energy E, the volume V, and the number of particles N are fixed) by molecular dynamics and Monte Carlo methods, cf. Refs. 10–12. Under these conditions, the equilibrium is *stable*, and the cluster size is defined by thermodynamic conditions $(\partial s/\partial g)_{E,V,N}=0$, $(\partial^2 s/\partial g^2)_{E,V,N}<0$, where s is the entropy; g, the number of atoms in the cluster. The equilibrium is reached by interchange of atoms between the cluster and vapor. In such a system, there is neither the size instability nor the critical radius.

In a real system under conditions of steady-state nucleation,[4] the pressure P and temperature T are fixed rather than E and V. A stable equilibrium is impossible, and cluster size at *unstable* equilibrium with the vapor (the critical size) is defined by the conditions[3] $(\partial\phi/\partial g)_{P,T,N}=0$, $(\partial^2\phi/\partial g^2)_{P,T,N}<0$, where ϕ is the Gibbs energy. These conditions are entirely different from that for the stable equilibrium. For this reason, the cluster thermodynamic quantities may be also different in (E,V) and (P,T) ensembles. Since the critical size is the most sensitive quantity, which defines the nucleation rate, a realistic simulation procedure is required, in which cluster evolution is investigated at $P,T=$const. Such a simulation makes it possible to record the critical size. Since the latter is much more sensitive to the size-dependent surface tension, this procedure could also serve as a test for various curvature corrections to the surface tension, in particular, for that proposed in Ref. 8.

In this work, a special procedure was developed to realistically simulate the vapor environment of a cluster. For this purpose, the surface of a simulation cell was a source of atoms that were randomly generated at any point of the surface in such a way that the cell was filled with a vapor with the Maxwell distribution over velocities corresponding to desired temperature and pressure. Atoms that crossed the surface were removed from the system. The cluster was placed in the center of the cell. Depending on initial cluster size, two types of evolution were observed. The larger clusters unlimitedly grew, the smaller ones were completely evaporated. In the region of intermediate initial sizes, which was attributed to the critical region, the cluster may occasionally increase or decrease in size.

More insight into the properties of clusters can be gained by studying their collective vibrations associated with density oscillations inside the cluster (phonons). For solidlike clusters, they are commonly known as breathing vibrations and are studied both theoretically[13–15] and experimentally.[16] Melting of a cluster results in dramatic changes in its phonon spectra, which appear to be intimately connected with a cluster evaporation mechanism. In this work, the spectral density of cluster potential energy per atom, which defines the evaporation rate, was analyzed at different stages of cluster evolution. Spontaneous emergence of breathing vibrations accompanied by a sharp increase of cluster evaporation rate was clearly observed in each run. This demonstrates that the collective vibration mechanism controls the evaporation rate rather than a conventional single-particle mechanism. Since the critical size is defined by the balance between condensation and evaporation, it depends on the phonon spectrum of a cluster as well. This feature can be used for the purposes of nucleation rate control and diagnostics of metal clusters.

The paper is organized as follows. In Sec. II, the system to be simulated and the simulation method are described in detail. The results of critical size determination are presented in Sec. III; cluster phonon spectra are analyzed in Sec. IV. The results obtained are discussed in Sec. V.

II. SIMULATION PROCEDURE

The system under investigation consisted of a cluster surrounded by supersaturated vapor. A spherical cell with the cluster placed in its center was chosen for simulations. A special numerical procedure maintained equilibrium distribution of vapor atoms over velocities with the constant temperature T_0 and average number of atoms N_v in the cell. For this purpose, the surface was made a source of randomly

generated atoms moving inward. At the same time, each atom approaching the surface from the inside was removed from the system. In this case, it is not necessary to include additional terms in the Hamiltonian of the system and impose kinematic constraints,[17] because P is not strictly fixed. Since the temperature is treated as a parameter, its instantaneous value defined by the system kinetic energy may fluctuate as well. Thus, only the *average* number of vapor atoms in the cell N_v is fixed. The vapor is assumed to be ideal, so $P=k_BT_0n_v$, where k_B is the Boltzmann constant; $n_v=N_v/V$; V is the cell volume.

Consider first the vapor generation procedure in absence of a cluster. The time evolution of a single-particle distribution function for vapor atoms $f(t,\mathbf{r},\mathbf{v})$ is described by the Boltzmann kinetic equation. If collisions inside the cell are neglected, it has the form $\partial f/\partial t+\mathbf{v}\cdot\nabla f=0$. The initial condition is $f(0,\mathbf{r},\mathbf{v})=0$, $|\mathbf{r}|<R$, where R is the cell radius (the origin of the coordinate system is placed in the center of the cell). The boundary condition is written in the form $f(t,\mathbf{R},\mathbf{v})=f_0(v)$ at $v_n<0$, where $v_n=\mathbf{v}\cdot\mathbf{R}/R$ is the normal velocity; $\mathbf{R}$, the radius vector of the point at the cell surface. Solution of the Boltzmann equation is

$$f(t,\mathbf{r},\mathbf{v})=\begin{cases}0, & t<\tau_r,\\ f_0(v), & t\geqslant\tau_r,\end{cases} \tag{1}$$

where $v\,\tau_r(\mathbf{r},\mathbf{v},R)=\rho+(\rho^2+R^2-r^2)^{1/2}$, $\rho=\mathbf{v}\cdot\mathbf{r}/v$. If the Maxwell distribution is used as the boundary condition, $f_0(v)=(n_v/\pi^{3/2}u^3)\exp(-v^2/u^2)$, where $u^2=2k_BT_0/M$, M is the atom mass, it is clear from solution (1) that the desired equilibrium distribution $f_0(v)$ is established in the entire cell within the vapor relaxation time $\tau_r\propto R/u$. Therefore, it is required that the number of atoms generated on the unit surface per unit time with velocities falling within the intervals (v_k,v_k+dv_k), $k=x,y,z$, is

$$dJ=-v_nf_0(v)dv_xdv_ydv_z. \tag{2}$$

The procedure of vapor generation comprised three stages. First, the point at the surface was chosen at random with uniform probability distribution. Second, three velocity components with probability distribution $p(v_k)=(1/\pi^{1/2}u)\exp(-v_k^2/u^2)$ were generated, and, third, an atom with this velocity was added to the system with probability $p_n=-4\pi v_n\tau n_vR^2/k_r$ if $v_n<0$, where τ is the molecular dynamics time step; k_r, the number of procedure repetitions per step ($k_r=2$ was adopted). Obviously, τ and R must be small enough and n_v low enough to provide that $p_n\sim4\pi u\,\tau n_vR^2/k_r\ll1$. In this case, a big number of time steps is required to create an atom, and generation is quasicontinuous. Thus, the desired number of atoms $dJ=p(v_x)p(v_y)p(v_z)p_ndv_xdv_ydv_zk_r/4\pi\tau R^2$ generated at each point of the surface is obtained [cf. Eq. (2)].

Consider now the procedure of cluster initialization. The simple cubic lattice was used to construct a cluster. The coordination number is closer to that in liquid argon for this lattice, unlike in the case of close packed lattice (e.g., fcc argon). Upon initialization, cluster atomic shells were successively filled until the desired number of atoms g was attained. Coordinates of the jth atom placed in the lth shell satisfied the conditions $x_j^2+y_j^2+z_j^2=la^2$, where x_j/a, y_j/a, and z_j/a are integers; a is the lattice period; $l=0,1,\ldots$. Each atom in the cluster was assigned three components of initial velocity with probability distribution $p(v_k)$. Cluster center-of-mass coordinates and velocity were then calculated and distracted from coordinates and velocities of each atom. Thus, the cluster with zero center-of-mass velocity was placed in the center of the cell.

The atoms were assumed to interact via the 12-6 Lennard-Jones potential $u(r_{ij})=4\epsilon[(\sigma/r_{ij})^{12}-(\sigma/r_{ij})^6]$, where $r_{ij}=|\mathbf{r}_i-\mathbf{r}_j|$; $\mathbf{r}_{i,j}$, the radius vectors of atoms. To simulate the interaction of the cluster with a thermostat (e.g., with a carrier gas), an additional term that stabilized cluster temperature was added to the expression for the force acting on an atom. The urgency of such a term follows from the fact that temperature fluctuations can essentially influence cluster evolution. In the absence of a thermostat, atom condensation on the cluster surface is associated with a considerable increase of cluster temperature $\Delta T\sim2q/3gk_B$, where q is the vaporization heat; evaporation decreases the temperature by the same amount. Since $q/k_BT_0\gg1$, it may be $q\Delta T/k_BT_0^2=2q^2/3gk_B^2T_0^2>1$ even at $\Delta T/T_0\ll1$. Thus, temperature fluctuations result in strong fluctuations of evaporation rate, which is proportional to $\exp(q\Delta T/k_BT_0^2)\gg1$. In such a way, condensation and evaporation appear to be strongly correlated. Indeed, as the temperature is increased after the condensation event, the evaporation probability increases; after evaporation it decreases. In addition, at the moments when the temperature is increased, the evaporation of dimers, trimers, etc., becomes possible, which indicates that the vapor is nonideal. Under these conditions, the temperature T_0 is no longer a good thermodynamic parameter of the system.

The term describing the interaction between the cluster and thermostat is written in the form of friction force, so the equation of motion for the jth atom is

$$\ddot{\mathbf{r}}_j=\frac{1}{\tau_0^2}\sum_{i\neq j}\left[2\left(\frac{\sigma}{r_{ij}}\right)^{14}-\left(\frac{\sigma}{r_{ij}}\right)^{8}\right](\mathbf{r}_j-\mathbf{r}_i)+\frac{1}{\tau_f}\left[\left(\frac{T_0}{T}\right)^{1/2}-1\right]\dot{\mathbf{r}}_j, \tag{3}$$

where $\tau_0=\sigma(M/24\epsilon)^{1/2}$ is the molecular dynamics time scale; τ_f, the temperature relaxation time; $T=(M/3gk_B)\Sigma_{j=1}^{g}\mathbf{v}_j^2$, the cluster temperature defined with the help of the equipartition theorem[17] ($\langle T\rangle=T_0$ at equilibrium, the angular brackets designate time averaging). The second term on the right-hand side of Eq. (3) (the friction term) enhances T if $T<T_0$ and vice versa. To ensure that the results of the simulation are independent of τ_f, its value must be sufficiently high, so that the second term on the right-hand side of Eq. (3) is much smaller than the first one. Otherwise, atom motion would be aperiodic. On the other hand, τ_f must be sufficiently small for temperature fluctuations to be small, $q\Delta T/k_BT_0^2<1$. Since the vapor atoms generated at the surface are produced by the thermostat itself, and their state must be independent of that of the cluster, it was set $\tau_f=\infty$ for vapor atoms.

A criterion is required to distinguish between vapor and cluster atoms. If the mean interatomic distance in the cluster is much less than that in the vapor, the following criterion proved to be useful, even if the cluster is shapeless. By defi-

nition, the atom belongs to the cluster if it has a neighbor within the distance r_b. It was demonstrated in Refs. 18 and 19 that average number of atoms in the cluster weakly depends on r_b if $r_b \propto \sigma$. To ascertain the value of r_b, minimum fluctuation of cluster size was required. It can be shown that this value corresponds to the turning point for the vapor atom in the potential of the cluster near its surface. Under the conditions specified in Sec. III, $r_b = 1.434\sigma$.

Due to collisions with vapor atoms, the cluster is involved in the Brownian motion that causes its slow drift toward the cell surface. To compensate this, the cell along with the coordinate system was periodically shifted to the cluster center-of-mass $\mathbf{r}_{\text{c.m.}}$. Coordinates of all atoms were transformed at the moment, when $r_{\text{c.m.}}^2 \geqslant R^2/12$. New coordinates and velocities were thus $\mathbf{r}_j' = \mathbf{r}_j - \mathbf{r}_{\text{c.m.}}$, $\mathbf{v}_j' = \mathbf{v}_j$. Atoms falling outside a new cell ($|\mathbf{r}_j'| > R$) were reflected symmetrically relative to the point $\frac{1}{2}\mathbf{r}_{\text{c.m.}}$, which preserved the total number of atoms. For these atoms, $\mathbf{r}_j' = -\mathbf{r}_j$, $\mathbf{v}_j' = -\mathbf{v}_j$.

The urgency of shifting the cell is related to the procedure of introduction of potential cutoff. Although no explicit cutoff is used in this work, finiteness of the cell radius R means that interaction with atoms beyond the cell is neglected. As was shown in Ref. 20, saturation vapor pressure obtained in molecular dynamics simulations of a flat interface between liquid and vapor is sensitive to r_c even at $r_c = 3\sigma$. The conditions of vapor generation $p_n \ll 1$ and the absence of collisions between vapor atoms ($R \ll n_v^{-1}\sigma^{-2}$) restrict R from above. All conditions are satisfied at the adopted value $R = 8\sigma$.

III. DETERMINATION OF CLUSTER CRITICAL SIZE

The set of Eq. (3) was integrated using the Verlet algorithm[17] with time step $\tau = 0.05$, where time is measured in the molecular dynamics time scale τ_0. The temperature was chosen to be equal to the melting temperature of real argon. At higher temperatures, the vapor becomes nonideal; at lower ones, numerical results cannot be compared with that of nucleation theories.

A desired supersaturation ratio $S = n_v/n_s(T_0)$, where $n_s(T_0)$ is the atom number density in the vapor at saturation, was fixed in each run. Since the value of n_s for real argon seems to be approached at $r_c \to \infty$ in molecular dynamics simulations (cf. Refs. 20 and 21), the experimental value[22] was adopted. In units of the values for an argonlike system[17] $\epsilon = 119.4$ K, $\sigma = 3.4 \times 10^{-8}$ cm, $T_0 = 0.7017\epsilon$, and $n_s(T_0) = 2.4 \times 10^{-3}\,\sigma^{-3}$.

In order to test the procedure of vapor generation, the temperature of the vapor $T_v = (M/3N_v k_B)\langle \Sigma_{j=1}^{N_v} \mathbf{v}_j^2 \rangle$ and its number density $\langle N_v \rangle / V$ were calculated at $S = 4$ during the generation for the cell without a cluster. These quantities were averaged over the time 10^4 and compared with desired values (T_0 and n_v, respectively). If the interaction between vapor atoms was ignored, calculated values converged to the desired ones. Otherwise, the temperature appeared to exceed T_0 by 4%, the number density was found to be 5% lower than n_v. These differences are indicative of vapor nonideality. The compressibility factor $PV/\langle N_v \rangle k_B T_v = 1 - \langle \Sigma_{i<j} r_{ij}(du/dr_{ij}) \rangle / 3\langle N_v \rangle k_B T_v$ was found to be equal to 0.95, which is somewhat higher than that for real argon due to the fact that the surface generator does not produce bound states of atoms. However, the equilibrium concentration of bound states is rather small in real argon. For example, the fraction of dimers is about 0.1 under these conditions, according to data.[22] Hence, the proposed generation procedure can provide reasonable accuracy in the simulation of a vapor.

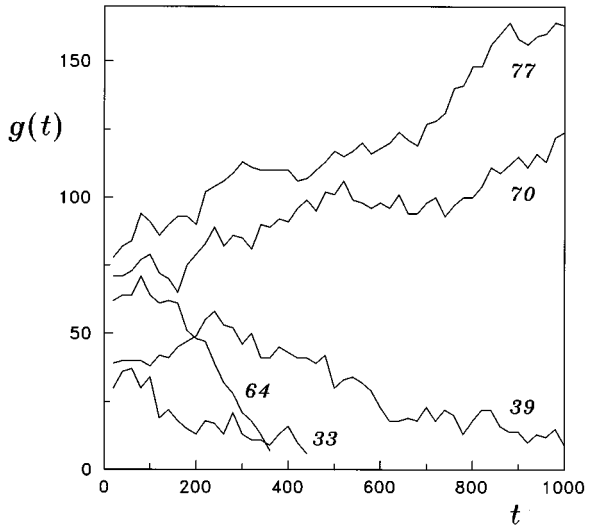

FIG. 1. Cluster size vs time for different initial sizes indicated at the right end of each curve.

Further calculations were performed for the cell containing a cluster. The cluster was initialized, and vapor generation began at $t = 0$. The run was terminated as soon as either the cluster was completely evaporated or its initial size was doubled. Numerical experiments were performed in two versions corresponding to $\tau_f = 0.125$ and $\tau_f = \infty$. Their results are much different. Thus, the average temperature fluctuation δT did not exceed 2–3 K for the first version (since $\delta T \tau_0 / 2 T_0 \tau_f \ll 1$, the "friction" force was still much weaker than interatomic interaction), and was as high as 20–30 K for the second one, so that the system could hardly be characterized by a certain temperature. As was pointed out in Sec. II, the higher the temperature fluctuations, the stronger the correlation between condensation and evaporation events. As a result, the time of complete cluster evaporation was $\sim 10^3$ in the first version and $\sim 10^4$ in the second one. The cell was filled with the vapor in a time $\tau_r \cong 65$. In order to decrease the loss of atoms by initialized cluster during this time, τ_f was set to infinity at $t < \tau_r$ even in the second version, so that the loss did not exceed three–four atoms.

Series of runs were performed in the first version for constant supersaturation $S = 4.4$ and different initial sizes $g(0)$. Figure 1 illustrates the phenomenon of size instability for typical size records. According to the initial size, the clusters can be divided in two groups. The ones with $g(0) < g^*$ evaporate and eventually disappear; the ones with $g(0) > g^*$ grow without limit. Here $g^* \cong 60$ is the critical size. Clusters with initial sizes about g^* occasionally join one of these groups, the width of the critical region being of the order 10. It is noteworthy that the amplitude of cluster size fluctuations is high even at nearly constant temperature.

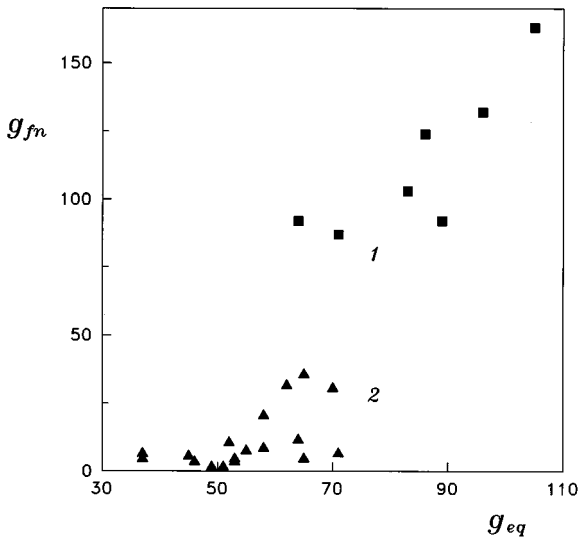

FIG. 2. Final cluster size $g_{\mathrm{fn}}=g(1000)$ vs equilibrium size $g_{\mathrm{eq}}=g(t_{\max})$. $S=4.4$; $\tau_f=0.125$. 1, supercritical clusters; 2, subcritical clusters.

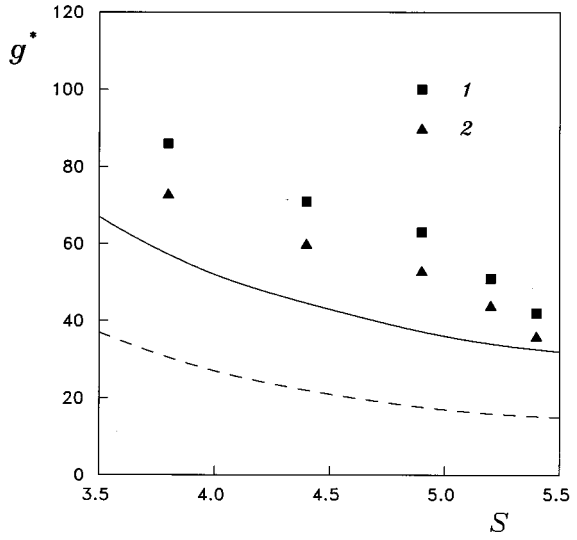

FIG. 3. Critical size vs supersaturation. The solid curve was calculated by formula (8) from Ref. 8; the dashed curve, by the classical nucleation theory (Ref. 4). Dots present molecular dynamics simulations: 1, supercritical clusters; 2, subcritical clusters.

Such fluctuations, which may considerably change the shape of cluster distribution over sizes, are not taken into account in the classical nucleation theory.

It can be seen in Fig. 1 that a decrease in size is preceded by growth for subcritical clusters [cf. $g(0)=39$ and 64], i.e., $g(t)$ passes through maximum at some $t=t_{\max}$ ($t_{\max}$ is varied from 80 to 350 in different runs), despite the fact that the vapor number density is lower than the stationary one at $t<\tau_r$. Supercritical clusters grow most quickly during this time. The change in cluster size is proportional to the difference between the fluxes of condensing and evaporating atoms. The first one is constant at fixed S. Therefore, the existence of such maximum means time lag in evaporation rate, which must be several times lower at $t<t_{\max}$ than at $t>t_{\max}$. It is shown further that this is a manifestation of the emergence of cluster phonons. Thus, $g_{\mathrm{eq}}=g(t_{\max})$ is always larger than $g(0)$. Cluster sizes at $t=1000$ are shown in Fig. 2. Two well-separated branches clearly indicate the size instability. The critical region is shifted toward larger sizes. The estimate $g^*\cong 68$ must be closer to the value of a real critical size.

Dependence of the critical size on supersaturation is shown in Fig. 3. Pairs of squares and triangles designate the upper and lower limits of the critical region. Each pair was obtained by several tens of runs at fixed S. The results of calculations using the classical nucleation theory and the theory[8] are also shown in Fig. 3. Required density, surface tension, and saturation pressure for argon were from Ref. 22; the dimer equilibrium constant was estimated using experimental PVT data: $K_p\cong -k_BT/MB\cong 26$ bar, where B is the second virial coefficient; the number of nearest neighbors in liquid argon is 10.5.

It can be seen that the classical nucleation theory yields the critical size, which is twice as low as that obtained in molecular dynamics simulations. It follows from estimates based on the theory[8] that the size correction to the surface tension is negative for argon, i.e., the critical size is larger than that in the classical nucleation theory. This qualitatively agrees with simulation results. It must be pointed out that there is no contradiction here with the results of other studies.[21] The Tolman length found in Ref. 21 is small and positive, but the size correction length δ in Ref. 8 is a different quantity. In any case, application of the Tolman correction factor $[1+2(g^*)^{-1/3}]^{-1}$ yields the unphysical result $g^*=1$.

It can be seen in Fig. 3 that the critical size found in molecular dynamics simulations decreases more quickly at $S>5$. At $S<3.8$, it deviates from the theory[8] toward larger sizes. Possible reasons for these effects may be as follows. The temperature is defined by the kinetic energy averaged over *all* bound atoms. By definition (Sec. II), the atom is assigned to the bound state if it has a neighbor within certain distance. Hence, colliding atoms are also assigned to the bound state. Since the kinetic energy of a pair of colliding vapor atoms exceeds the thermal one ($B<0$), the second term on the right-hand side of Eq. (3) decreases somewhat the temperature of a cluster. This effect must be more pronounced at small g (high S). In addition, the frequency of pair collisions in the cell increases as S^2. A decrease in cluster temperature results in a decrease of cluster evaporation rate, and, consequently, the critical size is decreased. At $S<3.8$, the critical size may be so large that the distance between its surface and the boundary of the cell is insufficiently large. In this case, the effect of the potential cutoff must increase the flux of evaporating atoms and, therefore, the critical size increases.

Simulations performed for the second version ($\tau_f=\infty$) showed that clusters with different sizes finally evaporated at supersaturations below the argon spinodal line, i.e., at $S<10$. At $S>10$, clusters grew regardless of their initial size. It is noteworthy that the average temperature of evaporating cluster appears to be several degrees *lower* than T_v. During positive temperature fluctuations, the evaporation probability is sharply enhanced, and evaporation of dimers and trimers is

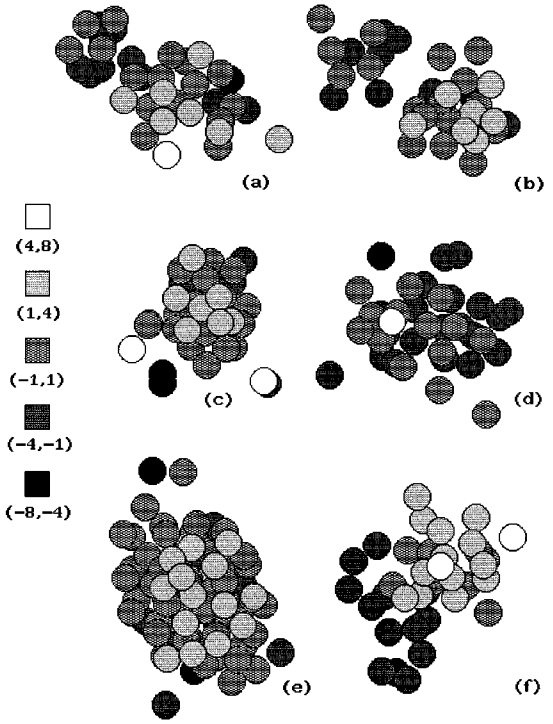

FIG. 4. Phases of cluster evolution: (a) and (b), evaporation of a 10-atom cluster; (c) and (d), the breathing vibrations, phases of ''expiration'' and ''breath'' are separated by 24 time units; (e), the lowest mode of the surface vibrations, $t=19.5$; (f), highly excited state with a chainlike structure. Fill styles designate coordinates of atoms with respect to the axis normal to the figure's plane. Corresponding intervals are indicated below the style types.

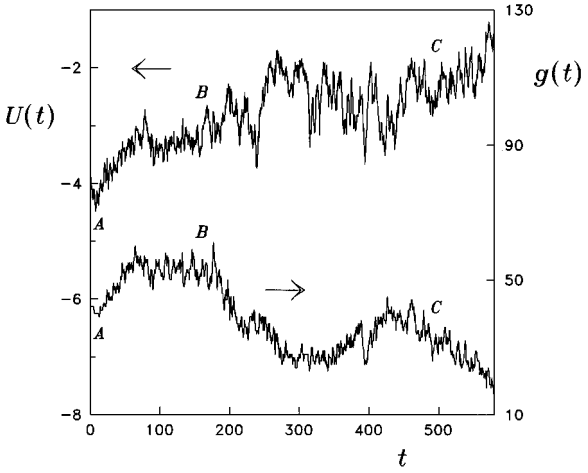

FIG. 5. Potential energy per atom and size of evaporating cluster as the functions of time. $S=4.4$; $\tau_f=0.125$.

observed. Such type of evolution agrees with well-known experimental fact: in the absence of a carrier gas, the nucleation is not favored.

Division of the cluster (or evaporation of dimers, trimers, etc., from its surface) was observed in the first version at $g<40$ as well. This can be understood with the help of the mass action law and the detailed balance equation. The higher the supersaturation, the smaller the critical size and the higher the equilibrium concentration of lightest clusters in the vapor. The rate of cluster division is proportional to this concentration, i.e., it increases as g decreases. Two sequential phases of cluster division are shown in Figs. 4(a) and 4(b).

It is noteworthy that clusters are such soft formations that atom elastic scattering on clusters are rather rare events, i.e., the accommodation coefficient is close to unity. In fact, vaporization energy released upon atom condensation is quickly dissipated by collisions with neighboring surface atoms. Typically, an incident atom is involved in vibrations with quickly decreasing amplitude in the neighborhood of the surface.

Three types of vibrations were observed in both versions of the simulation: the single-particle vibrations similar to that in bulk liquid with the shortest period of several time units; the breathing vibrations [Figs. 4(c) and 4(d)]; the surface vibrations similar to the capillary waves on the liquid surface [Fig. 4(e)]. The last two types are collective vibrations. Note that the surface vibrations, i.e., deformations of the cluster shape at constant interatomic distances, is a new vibration type that emerges as the cluster melts. A highly excited state of the ''breath'' phase is shown in Fig. 4(f). It can be seen that the cluster consists of several chains of atoms. The chainlike structure is also typical for the lightest clusters ($g<10$).

Different vibration types take different times for their development. Thus, single-particle vibrations emerge right after cluster initialization, development of the surface vibrations takes time about 20, the breathing vibrations are never observed at $t<t_{\max}$, i.e., at the time of the evaporation lag. This regularity allows us to assume that there is an intimate connection between breathing vibrations and evaporation rate. To investigate this phenomenon, cluster phonon spectrum was calculated.

IV. CLUSTER PHONON SPECTRUM

It is reasonable to refer the term phonon to collective vibrations even in the case of a liquidlike cluster, although no solidlike lattice exists in this case, and the phonons seem to be strongly coupled. Indeed, collective vibrations emerge spontaneously and have much in common with the sound in bulk liquid; their presence defines cluster properties. Thus, phonon means a certain type of vibration with a given energy. Since the interatomic distances in a cluster oscillate in collective vibrations, the spectrum of the sensitive quantity $U(t)=(gk_BT_0)^{-1}\Sigma_{i<j}u(r_{ij})$ was analyzed. In addition, U is proportional to cluster binding energy and is not much different from q/k_BT_0, the latter defining cluster evaporation rate.

About 40 runs for clusters initially containing 42 atoms were analyzed both in the first and second versions of the simulation. More or less pronounced, all the regularities discussed below were observed in each run. The time dependences $U(t)$ and $g(t)$ for the selected run are shown in Fig. 5. The run begins at the point A. The change in oscillation character can be noticed at the point B. In fact, oscillations of $U(t)$ have small amplitude at $t<t_B$, and $g(t)$ increases. At $t>t_B$, high-amplitude oscillations of $U(t)$ emerge, and $g(t)$ eventually decreases, that is, $t_B=t_{\max}=153$ is the evaporation time lag [the reason for the nonmonotonical behavior of

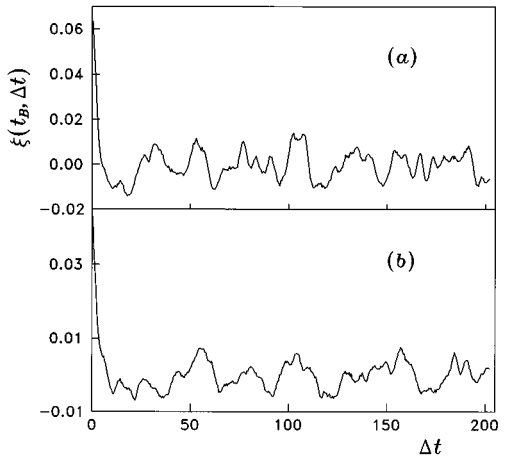

FIG. 6. Autocorrelation functions of $\tilde{U}(t)$ for the first (a) and second (b) versions of the simulation. $\theta=(t_C-t_B)/2$.

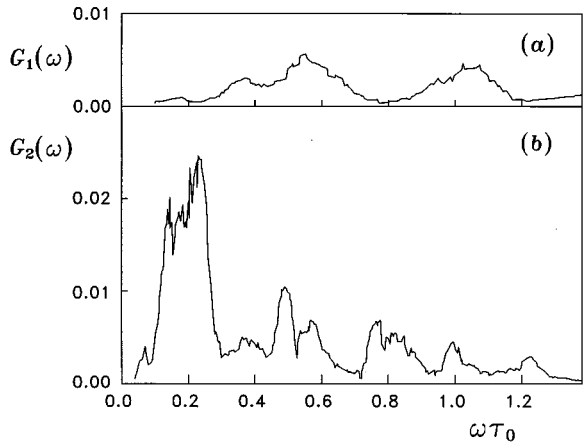

FIG. 7. Spectral densities of $\tilde{U}$ for the intervals AB (a) and BC (b), $\tau_f=0.125$.

$g(t)$ at $320<t<427$ is discussed in Sec. V]. At $t>t_C$, the cluster size is less than one-half of the initial size. The same regularity was observed for $\tau_f=\infty$, but the corresponding time scale is larger: for the second selected run, $t_B-t_A=440$, $t_C-t_B=630$.

First of all, the autocorrelation function was calculated for $U(t)$. This quantity was represented as the sum of the trend and the quickly oscillating component: $U=\bar{U}+\tilde{U}$. A considerable trend can distort the spectrum, therefore, $\tilde{U}(t)$ should be analyzed rather than $U(t)$. The trend $\bar{U}(t)$ is size dependent like all other cluster properties; this can be noticed in Fig. 5. Assuming that the cluster state is defined by the presence of phonons, one can approximate U by a linear time dependence. Thus, the intervals AB and BC are divided into several subintervals at points $t_i(t_i-t_{i-1}\gg 2\pi/\omega_0$, ω_0 is the characteristic oscillation frequency), so that $\bar{U}(t)=a_i+b_it$ at each subinterval. The points t_i and coefficients a_i, b_i were obtained by the least-squares fitting with the boundary conditions $a_{i+1}+b_{i+1}t_i=a_i+b_it_i$.

The time-dependent autocorrelation function is written in the form

$$\xi(t,\Delta t)=(\theta-\Delta t)^{-1}\int_t^{\theta+t-\Delta t}[\tilde{U}(t')-\langle\tilde{U}\rangle][\tilde{U}(t'+\Delta t)-\langle\tilde{U}\rangle]dt', \tag{4}$$

where $\langle\tilde{U}\rangle\equiv\theta^{-1}\int_t^{t+\theta}\tilde{U}(t')dt'$; θ is the time scale of local time averaging, which is here a substitution for ensemble averaging. Autocorrelation functions for the first and the second versions of simulation are shown in Fig. 6. The similarity of Figs. 6(a) and 6(b) shows that the observed vibrations are connected with cluster intrinsic properties and weakly depend on temperature fluctuation scale. It can be also seen that (i) the characteristic oscillation period is 15–60; (ii) no exact periodicity in Δt is observed; and (iii) the correlation time is greater than the cluster lifetime.

Standard methods of spectral analysis, in particular, the extensively used velocity autocorrelation function technique, are irrelevant here, because the treated process is nonstationary. Therefore, the conventional formula for spectral density $G(\omega)$ with ensemble averaging

$$G(\omega)=\lim_{\theta\to\infty}\left\langle\left|\theta^{-1}\int_0^{\theta}\tilde{U}(t)\exp\, i\omega t dt\right|^2\right\rangle$$

$$=\lim_{\theta\to\infty}\left[(2/\theta)\int_0^{\theta}\xi(0,t)\cos\,\omega t dt\right]$$

should be replaced by $G(\omega)=\langle|\tilde{U}_\omega(t)|^2\rangle$ with time averaging, where

$$\tilde{U}_\omega=t_1^{-1}\int_t^{t+t_1}\tilde{U}(t')\exp\, i\omega t' dt';\quad \omega=2\pi k/t_1;$$

$$k=1,2,\ldots \tag{5}$$

$G(\omega)$ is defined similar to autocorrelation function (4), the spectral density being assumed to be locally homogeneous in time. The functions $\tilde{U}_\omega$ are the coefficients of the discrete Fourier transform on the interval $(t,t+t_1)$; k is restricted from above by the condition $k\leqslant\omega_{\max}t_1/2\pi$, where $\omega_{\max}$ is the given maximum frequency. To make $\tilde{U}_\omega$ a quasicontinuous function of ω, the interval length t_1 is varied within the limits $\theta/2<t_1\leqslant\theta$ with step $\tau_\omega=0.5$ adjusted so that the spectral resolution (the average distance between two neighboring points on the frequency axis) $\delta\omega=(16\pi/3)(\tau_\omega/\theta^2)\ll\omega_{\min}$, where $\omega_{\min}=2\pi/\theta$ is the halfwidth of natural broadening of the spectral lines caused by the finiteness of cluster lifetime, $\omega_{\min}$ coincides with the minimum frequency attainable in the calculations. In other terms, each Fourier coefficient was calculated for a given t_1 and number k (i.e., for given frequency) at series of times t' on the interval $(t,t+\theta)$ and then the squared module of the coefficient was time averaged on this interval.

Vibrational spectral densities $G_{1,2}(\omega)=(2\delta\omega)^{-1}\int_{\omega-\delta\omega}^{\omega+\delta\omega}G(\omega')d\omega'$ averaged over spectral resolution are shown in Figs. 7 and 8. Subscripts 1 and 2 designate intervals AB and BC, respectively; corresponding values of θ are $(t_B-t_A)/2$ and $(t_C-t_B)/2$. A drastic difference between parts (a) and (b) can be seen in Figs. 7 and 8. In parts (a), only wide naturally broadened bands are observed. Sharp peaks with frequencies much lower than that of single-particle vibrations in parts (b) point to the fact that

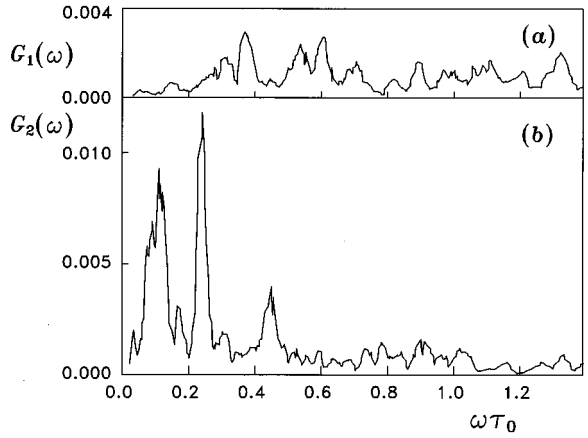

FIG. 8. The same quantities as in Fig. 7 for the second version of the simulation ($\tau_f=\infty$).

high-amplitude collective vibrations emerge at $t=t_B$. This is the evidence of the intimate connection between evaporation and breathing vibrations.

V. DISCUSSION

It can be seen in Figs. 7(b) and 8(b) that the three highest peaks in the low-frequency region have close frequencies: $\omega\tau_0=0.14$, 0.24, 0.48 and 0.11, 0.24, 0.45, respectively. Apparently, they must be of the same origin [the two highest peaks in Fig. 7(b) are badly resolved due to big natural line broadening]. Since the treated quantity $\tilde{U}(t)$ is most sensitive to average interatomic distance, one can attribute these peaks to breathing vibrations. Surface vibrations may also contribute to the spectrum, because they seem to be strongly coupled with breathing vibrations. In fact, the cluster prolate shape is associated with the ''expiration'' phase [Figs. 4(c) and 4(e)], and a slightly oblate shape with the ''breath'' phase [Figs. 4(d) and 4(f)], in contrast to the case of solidlike clusters.[13] The relatively weak dependence of vibrational frequencies on cluster size, which may be caused by vibration nonlinearity, is worth mentioning; corresponding line broadening does not exceed the natural one.

The following regularity in the peak arrangement can be seen in Figs. 7(b) and 8(b): the frequencies of the three highest peaks are in the ratio 1:2:4. They could not be associated with higher modes of breathing vibrations, because the corresponding ratio of frequencies would be that of odd numbers. The spectrum closely resembles that of a strange attractor,[23] in which energy transfer from high to low frequencies takes place.

Although vibrational spectra are very complicated, one conclusion is unambiguous: the onset of evaporation is connected with the emergence of vibrations with frequencies of about $(0.1–0.5)\ \tau_0^{-1}$, i.e., evaporation is a *collective* process. It is conventionally assumed that a single particle must have a kinetic energy greater than constant binding energy to evaporate. This is not true in the presence of phonons. Indeed, an increase of interatomic distances means a decrease of binding energy and vice versa. It can be seen in Fig. 5 that the oscillation amplitude may be as high as $2k_BT_0$. As a result, breath configurations [Fig. 4(d)] are favorable for the evaporation of single particles. The evaporation rate may be several times greater during this phase than during expiration [Fig. 4(c)]. Due to the strongly nonlinear exponential dependence of the evaporation rate on atom binding energy, a decrease in the latter may not be compensated for by its increase, and the net effect is evaporation enhancement. This demonstrates the dominant role of collective vibrations in evaporation.

Temporary cluster growth at $t>t_B$ (Fig. 5) does not seem to contradict this conclusion. In fact, the higher the cluster excitation, the higher the deformation at expiration. At $t=282$, the cluster becomes a shapeless prolate formation; the ratio of longitudinal to transverse dimension attains 4. Under these conditions, the cluster contains no atoms but the surface ones. With no inner atoms, the phonon must decay, and it takes time to restore it. This is a possible reason for a temporary decrease in the evaporation rate, which results in cluster growth.

Thus, the main regularities observed in this simulation are as follows. The rate of cluster evaporation and, therefore, its critical size are defined by the presence of phonons; this also defines cluster size fluctuations. The vibrational spectrum of liquidlike cluster resembles that of a strange attractor. Since no information specific for argon was involved in the simulations, it might be expected that the main regularities are of a universal nature. In the case of metal clusters, the interaction of phonons with the resonant electromagnetic field must enhance vibration amplitude and, therefore, the evaporation rate. Consequently, the critical size increases, and the nucleation rate must drop abruptly. This effect of radiation-induced inhibition of nucleation can be used for the purposes of nucleation rate control and diagnostics.

[1] R. Becker and W. Döring, Ann. Phys. **24**, 719 (1935).
[2] M. Volmer, *Kinetik der Phasenbildung* (Theodor Steinkopff, Dresden, 1939).
[3] J. Frenkel, *Kinetic Theory of Liquids* (Dover, New York, 1955).
[4] Ya. B. Zeldovich, JETP **12**, N11 (1942).
[5] H. Reiss, A. Tabazadeh, and J. Talbot, J. Chem. Phys. **92**, 1266 (1990).
[6] H. M. Ellerly and H. Reiss, J. Chem. Phys. **97**, 5766 (1992).
[7] C. L. Weakliem and H. Reiss, J. Chem. Phys. **101**, 2398 (1994).
[8] D. I. Zhukhovitskii, J. Chem. Phys. **101**, 5076 (1994).
[9] R. Mahnke, H. Urbschat, and A. Budde, Z. Phys. D **20**, 399 (1991).
[10] J. K. Lee, J. A. Barker, and F. F. Abraham, J. Chem. Phys. **58**, 3166 (1973).
[11] D. J. McGinty, J. Chem. Phys. **58**, 4733 (1973).
[12] A. I. Rusanov and E. Brodskaya, J. Colloid Interface Sci. **62**, 542 (1977).
[13] Y. Ozaki, M. Ichihashi, and T. Kondow, Chem. Phys. Lett. **182**, 57 (1991).
[14] R. E. Allen, G. P. Alldredge, and F. W. de Wette, Phys. Rev. B **4**, 1661 (1971).
[15] K. Kobashi and R. D. Etters, Surf. Sci. **150**, 252 (1985).
[16] U. Buck and R. Krohne, Phys. Rev. Lett. **73**, 947 (1994).
[17] D. W. Heerman, *Computer Simulations Methods in Theoretical Physics* (Springer, Berlin, 1986).
[18] K. Binder, J. Chem. Phys. **63**, 2265 (1975).
[19] M. Rao, B. J. Berne, and M. H. Kalos, J. Chem. Phys. **68**, 1325 (1978).
[20] M. J. P. Nijmeijer, A. F. Bakker, C. Bruin, and J. H. Sikkenk, J. Chem. Phys. **89**, 3789 (1988).
[21] M. J. Haye and C. Bruin, J. Chem. Phys. **100**, 556 (1994).
[22] N. B. Vargaftik, *The Reference Book on Thermophysical Properties of Gases and Liquids* (Nauka, Moscow, 1972).
[23] M. I. Rabinovich, Usp. Fiz. Nauk. **125**, N1 (1978).